Available online at www.sciencedirect.com

SciVerse ScienceDirect

Ceramics International 39 (2013) 5919–5924

CERAMICS INTERNATIONAL

www.elsevier.com/locate/ceramint

Hierarchical ZnO porous microspheres and their gas-sensing properties

Weiwei Guo[a,*], Tianmo Liu[a], Jinxing Wang[a], Weijie Yu[a], Rong Sun[b], Yong Chen[a], Shahid Hussain[a], Xianghe Peng[c], Zhongchang Wang[d]

[a]College of Materials Science and Engineering, Chongqing University, Chongqing 400044, PR China
[b]Institute of Engineering Innovation, The University of Tokyo, 2-11-16 Yayoi, Bunkyo-ku, Tokyo 113-8656, Japan
[c]Department of Engineering Mechanics, Chongqing University, Chongqing 400044, PR China
[d]WPI Research Center, Advanced Institute for Materials Research, Tohoku University, 2-1-1 Katahira, Aoba-ku, Sendai 980-8577, Japan

Received 26 November 2012; received in revised form 30 December 2012; accepted 7 January 2013
Available online 16 January 2013

Abstract

Materials with hierarchical and porous architectures often take on novel functional features. Here, we fabricate successfully the $Zn_4(OH)_6CO_3 \cdot H_2O$ (ZCHH) microspheres which consist of the nanoflakes by using a simple hydrothermal process, and demonstrate that the ZCHH precursor can be transformed utterly to ZnO porous microspheres after calcination. Further comparative studies reveal that both urea and MEA play a critical role in producing such unique porous microspherical architecture. The likely formation mechanism of the porous microspheres is proposed based on the time-dependent experiments. As a consequence of the unique hierarchical and porous architecture, the microspheres show a large specific surface area due to the remarkable amount of petals and pores on them and therefore excellent gas-sensing properties.

Keywords: D. ZnO; Crystal growth; Porous materials; Gas sensors

1. Introduction

With the large surface area, high porosity and low density, porous materials find many technological applications, in particular in the field of catalysis [1], gas sensing [2], transparent conductors [3], piezoelectricity [4] and photocatalysis [5]. These functionalities and associated potential applications are often affected by macroscopic morphology of the porous materials of interest and therefore great attentions have to date been exerted to the synthesis of porous materials. One representative example is the spherical porous particles and capsules which have superiority for application in drug delivery and release [6]. However, it remains technically difficult to control precisely the morphology of the porous materials, although such tuning has been successful in the silica-based porous materials [7]. The development of a simple yet efficient strategy to synthesize the porous materials with a tunable morphology still poses a significant challenge in modern synthesis science.

Being a chemically and thermally stable *n*-type semiconductor with high exciton binding energy (60 meV) and large band gap (3.37 eV), ZnO remains as one of the most hotly studied materials for a wide range of potential applications [8], especially when it appears in nano form. Among all of its applications, considerable interest has been devoted to its role as effective gas sensors by manipulating morphology of ZnO nanomaterials [9]. To date, a variety of porous ZnO nanostructures have been prepared successfully by means of many methods, including porous pyramids [10], porous nanotubes [11], mesoporous polyhedral cages [12], porous nanowires [13] and porous nanobelts [14], However, to best of our knowledge, the report on synthesis of pure porous ZnO microspheres remains scarce [15,16]. In this work, we demonstrate a successful synthesis of hierarchical ZnO porous microspheres *via* a facile and economical hydrothermal process, followed by annealing. Crystallinity, morphology and microstructure of the prepared microspheres are investigated, based upon which the

*Corresponding author. Tel.: +81 22 217 5933; fax: +81 22 217 5930.
E-mail addresses: shendaguowei@163.com (W. Guo), tmliu@cqu.edu.cn (T. Liu), zcwang@wpi-aimr.tohoku.ac.jp (Z. Wang).

0272-8842/$ - see front matter © 2013 Elsevier Ltd and Techna Group S.r.l. All rights reserved.
http://dx.doi.org/10.1016/j.ceramint.2013.01.014

likely formation mechanism is discussed. The prepared ZnO porous microspheres are found to exhibit good sensing performance to the ethanol gas.

2. Experimental

All chemical reagents were of analytical grade and used with no further purification. The zinc acetate dehydrate ($Zn(CH_3COOH)_2 \cdot 2H_2O$) (1 mM), urea (1 mM) and monoethanolamine (MEA) (0.3 mL) were first dissolved into distilled water (40 mL), followed by strong stirring for 1 h using magnetic stirrer. The solution was then transferred into autoclaves which were heated to 120 °C and maintained for 12 h. The formed zinc carbonate hydroxide hydrate precursors (ZCHH) white precipitate was washed thoroughly with distilled water to remove the residuals. Pristine ZnO porous microspheres were finally harvested by calcination of the ZCHH precursor at 450 °C for 2 h in air.

Microstructural analysis was conducted by the X-ray diffraction (XRD), scanning electron microscopy (SEM), and transmission electron microscopy (TEM). For the XRD, a Rigaku D/Max-1200X diffractometry with Cu Kα radiation operated at 40 kV and 200 mA was applied. Surface morphologies of the samples were observed using a Hitachi S-4300 SEM. Microstructure and chemical composition were further analyzed using the JEOL JEM-2010F electron microscope operated at an accelerating voltage of 200 kV. Specific surface area was calculated based upon the multipoint Brunauer–Emmett–Teller (BET) analysis of nitrogen adsorption isotherms, which were recorded using a surface area analyzer (Micromeritics, ASAP 2020M). Response of the sensors (S) was defined as the ratio of their resistances in air (R_a) to those in target gases (R_g) [2]. Response and recovery time was defined as the time taken by the sensors to achieve 90% of total resistance change during either the adsorption or the desorption process.

3. Results and discussion

3.1. Microstructural characterization

Fig. 1(a) shows XRD spectra of both the as-synthesized and calcined samples, from which the as-synthesized material is indexed as monoclinic $Zn_4(OH)_6CO_3 \cdot H_2O$ (JCPDS 11-0287) and the calcined one as well crystallized hexagonal ZnO (JCPDS 36-1451). No pronounced diffraction peaks of any other zinc-based compounds are seen, indicating that the precursor is transformed to pure ZnO after calcination. Fig. 1(b)–(f) shows the representative SEM and TEM images of the ZCHH precursor after calcination at 450 °C for 2 h in air. From Fig. 1(b) and (c), the obtained ZnO particles are found to take form of monodispersed microspheres with an average size of 1–2 μm. An enlarged SEM image of an individual microsphere is shown in Fig. 1(d), from which the microsphere is found to be constructed of numerous nanoflakes that are interweaved together. These nanoflakes form an open porous structure. The TEM image of a fringe region of an individual microsphere is shown in Fig. 1(e), which further reveals that the three-dimensional porous microsphere is assembled by the two-dimensional nanoflakes with thickness of 12–30 nm. Numerous irregular pores with a size of 5–50 nm are randomly distributed in the nanosheets (Fig. 1(f)), which is attributed to evaporation of volatile gas such as H_2O and CO_2 during the heat treatment.

3.2. Growth mechanism of ZnO porous microspheres

To gain insight into the growth mechanism and the role played by the additives during the synthesis, we conduct SEM investigations with a special focus on change of morphology in the synthesized samples as a function of the introduced additives. As seen in Fig. 2(a), large-sized flake-like ZnO particles are generated by adding the urea only. However, when it is changed to the monoethanolamine (MEA), smaller ZnO nanoparticles and clusters are formed (Fig. 2(b)), indicating that the additives are key to the formation of porous microspheres. The urea is hence speculated to promote the growth of ZCHH flakes, while the MEA restrains the nanocrystals from forming large-sized flakes, thereby accelerating the assembling of flake-like nanocrystals into spheres.

To further reveal the evolution process, we prepare the ZnO samples at different reaction times followed by calcination at 450 °C and observe the SEM images of the samples. The ZnO sample prepared at 1 h is found to be composed of thin nanoflakes and nanoflake clusters (Fig. 2(c)). These nanoflakes and clusters start to recrystallize and assemble to small microspheres when the hydrothermal reaction time is increased to 4 h (Fig. 2(d)). When further increasing hydrothermal time, the three-dimensional porous microspheres grow continually both in size and quantity. The uniform porous microspheres are obtained as the time is set to 12 h (Fig. 2(e)). Further increase in the hydrothermal time to 20 h renders some nanoflakes dissolved and some spheres even collapsed (Fig. 2(f)), indicating that over treatment process is adverse to the formation of sphere structures.

Fig. 3 illustrates schematically the formation process of porous microspheres in light of the aforementioned experimental observations. At initial stage, the ZCHH nanocrystals are produced randomly after introducing the urea (see Eqs. (1)–(4)). With the rise of reaction time, the ZCHH colloids are aggregated to form nanoflakes *via* the oriented attachment mechanism [17]. When the MEA is dispersed uniformly in the solution, there forms the coordinated $[Zn(MEA)m]^{2+}$ ions (where m is an integer) [18], which limits the number of free Zn^{2+} ions and the ZCHH colloids. This process restrains the nanoflakes from growing. As the hydrothermal reaction time continues to rise, the ZCHH nanoflakes are self-aggregated to eliminate

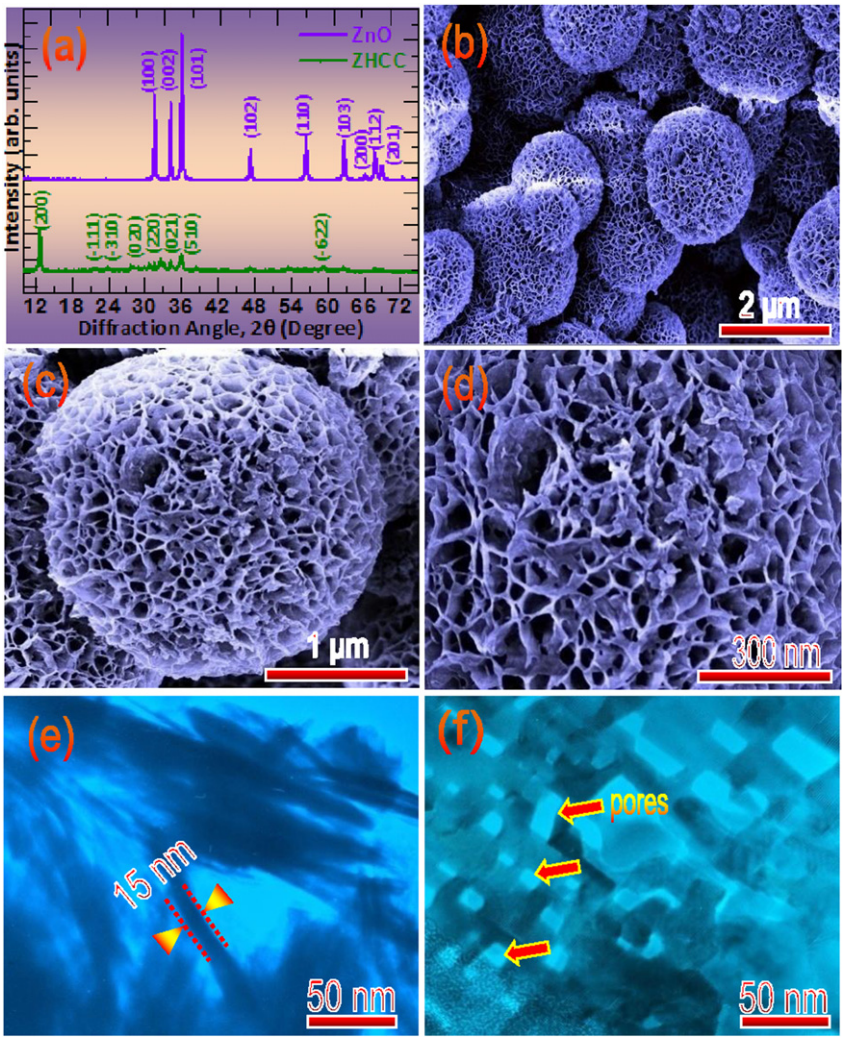

Fig. 1. (a) XRD spectra of the ZHCC precursor and the porous ZnO microspheres. (b–d) SEM images of the porous ZnO microspheres. (e) and (f) TEM images of a fringe region of individual ZnO microsphere.

their surface energy [19], forming the nanoflake clusters which eventually evolve into the porous microspheres.

$$(NH_2)_2CO + H_2O \rightarrow 4NH_3 + CO_2 \quad (1)$$

$$NH_3 + H_2O \leftrightarrow NH_4^+ + OH^- \quad (2)$$

$$CO_2 + H_2O \leftrightarrow CO_3^{2-} + 2H^+ \quad (3)$$

$$4Zn^{2+} + CO_3^{2-} + 6OH^- + H_2O \rightarrow Zn_4(OH)_6CO_3 \cdot H_2O \quad (4)$$

$$Zn^{2+} + m\mathrm{MEA} \leftrightarrow [Zn(\mathrm{MEA})m]^{2+} \quad (5)$$

Fig. 4(a) shows the response to ethanol gas of 50 ppm as a function of the operating temperature ranging from 200 to 500 °C for the three sensors made of the ZnO nanoparticles, nanoflakes and porous microspheres. The highest value of gas response for the nanoparticles, nanoflakes and nanoflowers is estimated to be 21.9, 39.6 and 87.5, respectively. The optimal operating temperature for the three sensors is determined to be 350 °C. Clearly, the sensor made of the porous microspheres shows the strongest response to ethanol at almost all the tested temperatures, indicating that morphology of porous microspheres is critical for further enhancement of gas-sensing properties of ZnO. The BET surface area of the nanoparticles, nanoflakes and porous microspheres is calculated to be 4.9, 3.7 and 39.6 $m^2 g^{-1}$, respectively, suggesting that the porous microspheres have the largest specific surface area. Such a unique porous and hierarchical structure with the largest specific surface area should be responsible for the enhancement of gas response because the adsorption of target gas molecules should be accelerated with this structure. The response and recovery time for the three sensors operated in the ethanol gas of 50 ppm at 350 °C is shown in Fig. 4(b). In light of the aforementioned definition, the response and recovery time is evaluated to be 19 and 20 s for the nanoparticles, 12 and 14 s for the nanoflakes, and 7 and 9 s for the microspheres. As a consequence of the unusual microstructure, the sensor made of the microspheres exhibits the shortest response and recovery time, implying that the adsorbed gas molecules can be desorbed away from the sphere surface in the least

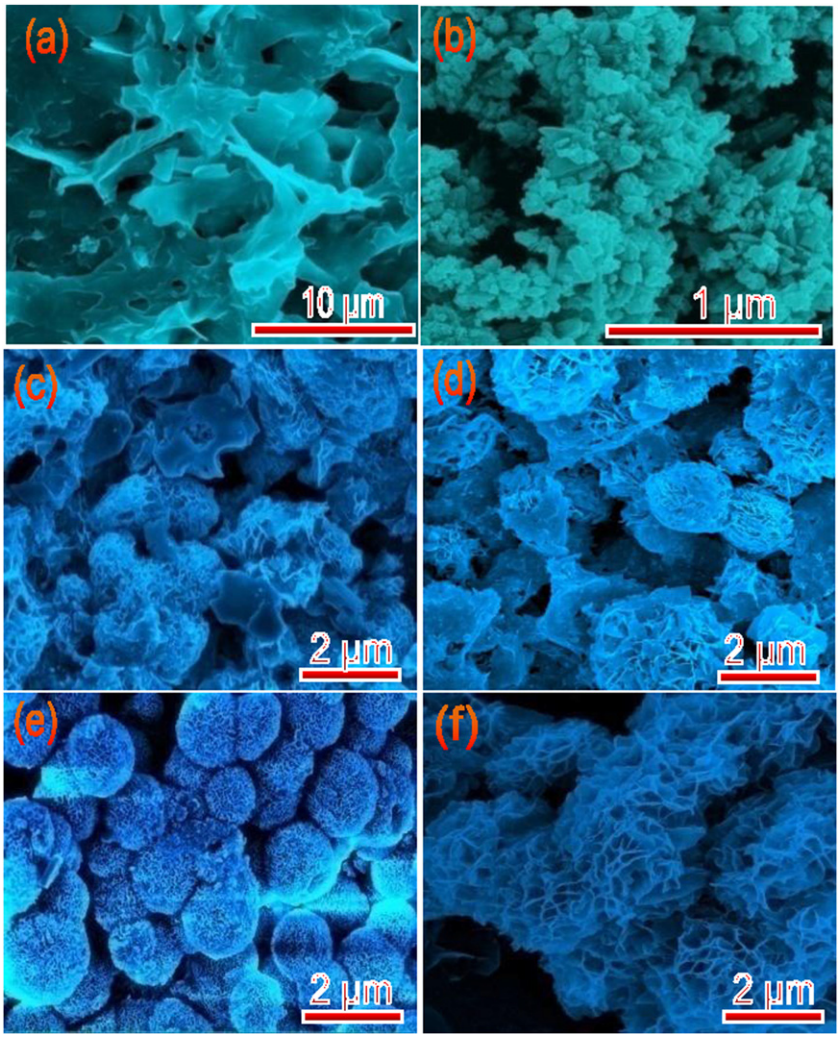

Fig. 2. SEM images of the ZnO samples prepared by introducing (a) urea alone and (b) MEA alone. SEM images of ZnO microspheres prepared at (c) 1 h, (d) 4 h, (e) 12 h and (f) 20 h, followed by calcination treatment at 450 °C.

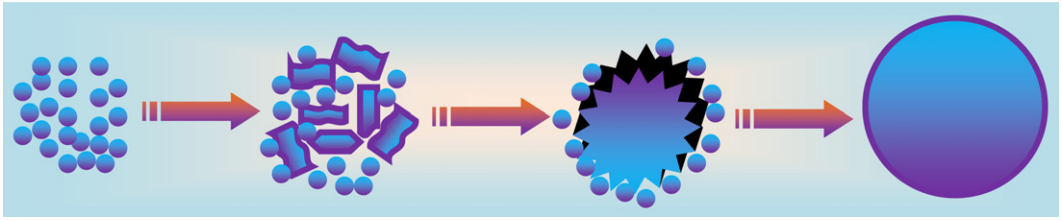

Fig. 3. Schematic plot illustrating the evolution of the porous ZnO microspheres.

difficult manner. This might be because on one hand, the porous microspheres has a significant amount of small and free-following tunnels for absorption and desorption, and on the other hand, the nanoflakes, which act as building blocks for microspheres, bear many mesopores as well.

The gas-sensing mechanism of ZnO can be understood upon the surface charge model. When exposed in different type of gases, resistance of semiconductor oxide materials alters [20,21]. When the sensor is first exposed in air, oxygen molecules in the atmosphere are chemically absorbed on ZnO surfaces (such as O^{2-}, O^{-} and O^{2-}), resulting in surface electron depletion layer [22,23]. As the absorption process reaches equilibrium, the gas-sensing materials take on a high resistivity due to the depletion of carriers on the surface. On the other hand, when exposed in reduced atmosphere (e.g., in the ethanol gas), the gas molecules interact with the chemisorbed oxygen on the surface, which releases the electrons back to the semiconductor. This

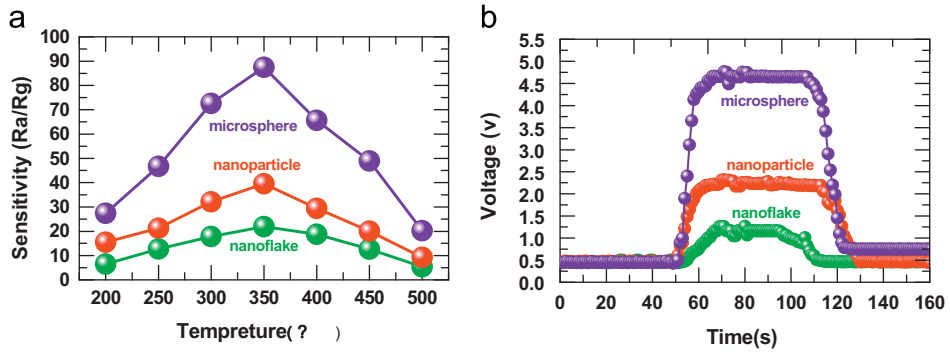

Fig. 4. (a) Gas response of the sensors made of the ZnO particles with three different morphologies to the ethanol of 50 ppm measured at temperature ranging from 200 to 500 °C. (b) Response and recovery transients of the sensors made of the ZnO powders with different morphologies to the ethanol of 50 ppm. The measurement temperature is fixed to 350 °C.

indicates that the electron concentration increases and as a consequence the resistance of the materials decreases.

4. Conclusions

We have successfully prepared hierarchical ZnO porous microspheres with an average size of 1–2 μm *via* the simple yet efficient hydrothermal approach followed by calcination of the ZCHH precursor. The role of the additives on the morphology of the samples is investigated and gas-sensing properties of the fabricated samples are examined. We find that the urea additive promotes the formation of nanoflakes and that the MEA enables shrinking of the nanoflakes and easier assembling of nanoflakes to spheres. A possible growth mechanism is proposed based upon the experimental observations. Further gas-sensing measurements reveal that the sensor made of porous ZnO microspheres exhibits the highest gas response (87.5) and the shortest response and recovery time (7 and 9 s, respectively) to the ethanol gas of 50 ppm at an optimal temperature of 350 °C.

Acknowledgments

This work was supported by the Natural Science Foundation Project of CQ CSTC under Grant no. 2010BB4054.

References

[1] H.P. Liang, H.M. Zhang, J.S. Hu, Y.G. Guo, L.J. Wan, C.L. Bai, Pt hollow nanospheres: facile synthesis and enhanced electrocatalysts, Angewandte Chemie International Edition 43 (2004) 1540–1543.
[2] W.W. Guo, T.M. Liu, W. Zeng, D.J. Liu, Y. Chen, Z.C. Wang, Gas-sensing property improvement of ZnO by hierarchical flower-like architecture, Materials Letters 65 (2011) 3384–3387.
[3] Y. Imanishi, M. Taguchi, K. Onisawa, Effect of sublayer surface treatments on ZnO transparent conductive oxides using dc magnetron sputtering, Thin Solid Films 518 (2010) 2945–2948.
[4] X. Wang, J. Song, J. Liu, Z.L. Wang, Direct-current nanogenerator driven by ultrasonic waves, Science 316 (2007) 102–105.
[5] K. Liu, M. Sakurai, M. Aono, ZnO-based ultraviolet photodetectors, Sensors 10 (2010) 8604–8634.
[6] Y. Zhu, T. Ikoma, N. Hanagata, S. Kaskel, Rattle-type Fe_3O_4@SiO_2 hollow mesoporous spheres as carriers for drug delivery, Small 6 (2010) 471–478.
[7] S.W. Kim, M. Kim, W.Y. Lee, T. Hyeon, Fabrication of hollow palladium spheres and their successful application to the recyclable heterogeneous catalyst for suzuki coupling reactions, Journal of the American Chemistry Society 124 (2002) 7642–7643.
[8] Z.Y. Fan, J.G. Lu, Zinc oxide nanostructures: synthesis and properties, Journal of Nanoscience. and Nanotechnology 5 (2005) 1561–1573.
[9] W.W. Guo, T.M. Liu, H.J. Zhang, R. Sun, Y. Chen, W. Zeng, Z.C. Wang, Gas-sensing property performance enhancement in ZnO nanostructures by hierarchical morphology, Sensors and Actuators B 166–167 (2012) 492–499.
[10] Z.H. Dai, K. Liu, Y.W. Tang, X.D. Yang, J.C. Bao, J.J. Shen, A novel tetragonal pyramid-shaped porous ZnO nanostructure and its application in the biosensing of horseradish peroxidase, Journal of Materials Chemistry 18 (2008) 1919–1926.
[11] H.Q. Wang, G.H. Li, L.C. Jia, G.Z. Wang, C.J. Tang, Controllable preferential-etching synthesis and photocatalytic activity of porous ZnO nanotubes, The Journal of Physical Chemistry C 112 (2008) 11738–11743.
[12] P.X. Gao, Z.L. Wang, Mesoporous polyhedral cages and shells formed by textured self-assembly of ZnO nanocrystals, Journal of American Chemical Society 125 (2003) 11299–11305.
[13] C.X. Shan, Z. Liu, Z.Z. Zhang, D.Z. Shen, S.K. Hark, A simple route to porous ZnO and ZnCdO, The Journal of Physical Chemistry B 110 (2006) 11176–11179.
[14] Z. Gui, J. Liu, Z.Z. Wang, L. Song, H. Yuan, W.C. Fan D.Y. Chen, From multicomponent precursor to nanoparticle nanoribbons of ZnO, The Journal of Physical Chemistry B 109 (2005) 1113–1117.
[15] P.T. Zhao, J.T. Fan, Fabrication of the flower-like $Zn_5(OH)_6(CO3)_2$ and ZnO microstructures consisting of the dendritic nanosheets, Materials Letters 83 (2012) 115–117.
[16] J.F. Li, G.Z. Lu, Y.Q. Wang, Y. Guo, Y.L. Guo, A high activity photocatalyst of hierarchical 3D flowerlike ZnO microspheres: synthesis, characterization and catalytic activity, Journal of Colloid and Interface Science 377 (2012) 191–196.
[17] N. Markus, C. Helmut, Oriented attachment and mesocrystals: non-classical crystallization mechanisms based on nanoparticle assembly, Physical Chemistry Chemical Physics 8 (2006) 3271–3287.
[18] X.J. Wang, Q.L. Zhang, Q. Wan, G.Z. Dai, C.J. Zhou, B.S. Zou, Controllable ZnO architectures by ethanolamine-assisted hydrothermal reaction for enhanced photocatalytic activity, Journal of Physical Chemistry C 115 (2011) 2769–1775.
[19] P. Hu, X. Zhang, N. Han, W.C. Xiang, Y.B. Cao, F.L. Yuan, Solution-controlled self assembly of ZnO nanorods into hollow microspheres, Crystal Growth and Design 11 (2011) 1520–1526.

[20] M. Egashira, Y. Shimizu, Y. Takao, S. Sako, Variations in *I–V* characteristics of oxide semiconductors induced by oxidizing gases, Sensors and Actuators B 35 (1996) 62–67.

[21] W. Zeng, T.M. Liu, Z.C. Wang, Impact of Nb doping on gas-sensing performance of TiO_2 thick-film sensors, Sensors and Actuators B 166–167 (2012) 141–149.

[22] N. Hongsith, E. Wongrat, T. Kerdcharoen, S. Choopun, Sensor response formula for sensor based on ZnO nanostructures, Sensors and Actuators B 144 (2010) 67–72.

[23] W. Zeng, T.M. Liu, Z.C. Wang, Enhanced gas-sensing properties by SnO_2 nanosphere functionalized TiO_2 nanobelts, Journal of Materials Chemistry 22 (2012) 3544–3548.